Proceedings of Science and Mathematics
Faculty of science, universiti teknologi malaysia
https://science.utm.my/procscimath/
Volume 29 (2025) 6-17

Discovery of Antimicrobial Resistance Counteragents via Virtual Screening and Structure-Activity Relationship Analysis

Christina Kow Yong Xin[a], Tayal Punitha Ramasamy Naidu[a], Nurzila Ab Latif[a], Norazah Basar[b], Syazwani Itri Amran[a]*

[a] Department of Biosciences, Faculty of Science, Universiti Teknologi Malaysia, 81310 Johor Bahru, Johor, Malaysia.

[b] Department of Chemistry, Faculty of Science, Universiti Teknologi Malaysia, 81310 Johor Bahru, Johor, Malaysia.

*Corresponding author: syazwaniitri@utm.my

Abstract

Antimicrobial resistance (AMR) poses a growing global health threat, particularly due to multidrug-resistant pathogens like carbapenem-resistant *Acinetobacter baumannii*. To accelerate drug discovery, this study employed a comprehensive *in silico* approach targeting two key resistance-related enzymes: PBP 1a (PDB ID: 3UDX) and β-lactamase (PDB ID: 5L2F). Twenty phytochemicals (C1-C20) derived from *Persea fruticosa* were sketched and geometrically optimised using Avogadro software. These compounds were then docked against both proteins using AutoDockTools v1.5.7. Although none surpassed the binding affinities of the control ligands (IM2 and 4J6), compounds C4, C13, C18, and C20, with the most favourable docking scores, were selected for further analysis. Structure-Activity Relationship (SAR) analysis revealed that the library compounds exhibited weaker hydrogen bonding and hydrophobic interactions compared to controls. Structural modifications were then applied to C4, C18, and C20, resulting in modC4, modC18, and modC20, which demonstrated improved docking scores and binding interactions. Further *in silico* evaluations showed modC4 and modC18 complied with Lipinski's rule of five and had favourable ADMET properties, suggesting potential for intravenous administration. In contrast, modC20 violated key drug-likeness parameters. This study underscores the effectiveness of *in silico* methods in identifying and optimising potential antimicrobial agents against resistant pathogens.

Keywords: Antimicrobial resistance; *Acinetobacter baumannii*; Penicillin binding protein; β-lactamase; Molecular docking

Introduction

In recent years, antimicrobial resistance (AMR) has become one of the global threats in the 21st century, and it could be the primary cause of death worldwide if preventive measures are not available by 2050 (Tang et al., 2023). While AMR can arise naturally through gene mutations or horizontal gene transfer (HGT), its spread has been significantly accelerated by the misuse and overuse of antibiotics. In 2021 alone, AMR was linked to approximately 4.71 million deaths, contributing to increased morbidity, mortality, and healthcare costs (Naghavi et al., 2024).

This issue is further complicated by ESKAPE pathogens (*Enterococcus faecium, Staphylococcus aureus, Klebsiella pneumoniae, Acinetobacter baumannii, Pseudomonas aeruginosa, and Enterobacter* spp.), which have acquired multiple resistance genes and are increasingly difficult to treat (De Oliveira et al., 2020). In recognition of the urgency, the World Health Organization (WHO) identified AMR as one of the top 10 global health threats and listed the bacterial priority pathogens into three different groups: critical, high and medium. Notably, carbapenem-resistant *Acinetobacter baumannii* (CRAB), which falls under the critical category, poses a serious clinical challenge due to its high resistance to carbapenems—antibiotics often reserved as a last line of defence.

In Malaysia, the resistance rate of *A. baumannii* to carbapenems has risen alarmingly from 49% in 2008 to 68.8% in 2021 (Ministry of Health Malaysia, 2022). This resistance is largely mediated by the production of β-lactamase enzymes, which hydrolyse the β-lactam ring of carbapenems before the drug can reach its target (Zango et al., 2019). Normally, β-lactam antibiotics exert their effect by binding to penicillin-binding proteins (PBPs), essential enzymes that catalyse the transpeptidation reaction during bacterial cell wall synthesis. However, in the presence of functional β-lactamase, these antibiotics are inactivated, allowing PBPs to proceed with peptidoglycan cross-linking and enabling bacterial survival despite antibiotic treatment.

Given the time-consuming, labour-intensive, and costly nature of traditional drug discovery, computer-aided drug design (CADD) has become an attractive alternative to accelerate the identification of effective antimicrobial agents. Techniques such as virtual screening, molecular docking, quantitative structure–activity relationship (QSAR) modelling, and *in silico* ADMET (Absorption, Distribution, Metabolism, Excretion, and Toxicity) profiling enable rapid and cost-effective screening of large compound libraries, allowing researchers to prioritise promising candidates for further experimental validation.

In this study, computational tools were used to identify and optimise novel antimicrobial compounds targeting penicillin-binding protein (PBP) and β-lactamase in *A. baumannii*. Both enzymes play key roles in cell wall biosynthesis and β-lactam antibiotic resistance, making them attractive therapeutic targets. Through integrated virtual screening, molecular docking, SAR analysis, and ADMET evaluation, this research aims to discover phytochemical-derived compounds with strong binding affinity and favorable pharmacokinetic properties suitable for further development.

Materials and methods

The protein preparation involved retrieving the structures of target penicillin-binding protein 1a (PBP1a) (PDB ID: 3UDX) and β-lactamase (PDB ID: 5L2F) from A. *baumannii* from the Protein Data Bank (PDB) (https://www.rcsb.org/) and their 3D structures were downloaded in .pdb format (Han et al., 2011; June et al., 2016). Additional chains, stabilizers (glycerol and acetate ion) and water molecules were removed from the protein crystal structure, followed by adding polar hydrogen atoms. The co-crystal ligand was then removed from the protein structure and both protein and ligand structures were saved in .pdb format separately.

The 3D structures of phytochemicals extracted from *Persea fruticosa* were sketched using Avogadro software based on the 2D structures obtained from liquid chromatography-mass spectrometry (LCMS) data。 The initial energy of the 3D ligand structures was obtained using the Calculate Energy setting from the Molecular Mechanics wizard. Subsequently, the 3D structures were geometrically optimized using the Optimize Geometry function.

Control docking was carried out between the protein and its co-crystal ligand to identify the coordinates of the binding site using the AutoDock Tools (ADT) v1.5.7 program. The grid parameters for docking were then set by defining a grid box centered on the ligand binding site. A grid box dimension with a 40 × 40 × 40 dimension was created. The coordinates obtained for PBP (PDB ID: 3UDX) and β-lactamase (PDB ID: 5L2F) were (-35.409, -3.419, -11.753) and (-9.983, -23.426, 39.481), respectively. Following this step, molecular docking was carried out by executing AutoDock4, with the number of runs and population size adjusted to 20 and 150, respectively, in the Genetic Algorithm parameter. The docking process produced a .dlg file that contains 20 conformations of the ligand along with their respective estimated free binding energies and estimated inhibition constants.

A similar procedure was repeated for the analysis of the compound library using the coordinates determined from the control docking previously. Molecular docking was conducted with the number of runs increased to 50 while maintaining a population size of 150. Next, binding affinity and structure-activity relationship (SAR) analyses of the docking results were performed using PyMOL v3.1 and Biovia Discovery Studio Visualizer. PyMOL was used to compare the docking poses with co-crystal ligands to confirm binding orientation, while Discovery Studio Visualizer was used to examine key interactions such as hydrogen bonds, hydrophobic contacts, and pi-stacking between the ligands and the target proteins.

Based on SAR analysis, key pharmacophores such as hydrogen bond donors/acceptors, hydrophobic groups, and aromatic rings were identified by comparing selected hits with control compounds (IM2 and 4J6). These features were added to hit compounds using Avogadro software to improve their binding to PBP 1a and β-lactamase. The modified compounds were energy-minimized in Avogadro and saved in .pdb format for redocking.

The SMILES codes of the modified compounds were then submitted to the SwissADME server (http://www.swissadme.ch/) to assess pharmacokinetics and druglikeness properties. Key parameters for pharmacokinetic properties included molecular weight, GI absorption, BBB permeability, CYP inhibition, and skin permeability, while druglikeness was evaluated using Lipinski's rule of five.

Results and discussion

Control docking was performed to validate the docking procedure and identify the coordinates of the ligand-binding site by redocking the co-crystallized ligands (IM2 and 4J6) against their respective target proteins (PBP 1a and β-lactamase). Model 5 was selected as the best docking model for IM2/PBP 1a complex with a binding energy value of -6.05 kcal/mol and root mean square deviation (RMSD) value of 2.89 Å. Meanwhile, the lowest binding energy for the 4J6/β-lactamase complex was observed in model 3, with a binding energy of -9.48 kcal/mol and root mean square deviation (RMSD) of 2.20 Å. Although RMSD values below 2.0 Å are typically indicative of excellent docking results, values ranging from 2.0 to 3.0 Å are also considered acceptable, especially for ligands with a high number of rotatable bonds, implying high flexibility of the ligand structure.

To further validate the docking accuracy, the selected models were superimposed with their respective crystal structures, as illustrated in Figure 1. The superimposition of the IM2/PBP 1a complex revealed a noticeable deviation in ligand orientation compared to the original co-crystallized structure, suggesting possible flexibility in the active site. In contrast, the docking model for the 4J6 complex closely mimicked the binding orientation of its co-crystal ligand, supporting the reliability of the docking protocol.

Table 1: Control docking result of co-crystallized ligands (IM2 and 4J6) against their respective target proteins (PBP 1a and β-lactamase).

Ligand/protein complex	Best docking model	Binding energy (kcal/mol)	RMSD (Å)
IM2/PBP1a complex	Model 5	-6.05	2.89
4J6/β-lactamase complex	Model 3	-9.48	2.20

Following molecular docking analysis, the estimated binding free energy and inhibition constant for each compound against both PBP 1a and β-lactamase were extracted from the .dlg files generated by AutoDock v4.2.6. The docking results of library compounds against PBP 1a (PDB ID: 3UDX) and β-lactamase were summarized in Tables 2 and 3, respectively.

From Table 2, none of the library compounds demonstrated binding free energies or inhibition constants comparable to the control compound (IM2). However, four compounds (C20, C4, C18, and C13) recorded binding free energies that were approximately one order of magnitude lower than that of IM2, indicating relatively weaker binding. To further investigate their binding behaviour, superimposition analysis was performed for these four compounds. As shown in Figure 2 (a), C20 exhibited the lowest binding free energy (-5.65 kcal/mol) among the library compounds, likely due to its partial spatial overlap and slightly similar orientation to IM2, contributing to its more favourable binding free energy and enhanced affinity to PBP 1a. In contrast, C4 and C18 did not exhibit significant overlap with IM2 and adopted noticeably different orientations, as illustrated in Figures 2 (b) and (c). Although C13 displayed slight spatial overlap with IM2, its aromatic ring was oriented most distantly and differently from that of IM2, as shown in Figure 2 (d). This misalignment likely resulted in the loss of key hydrogen bond interactions with surrounding residues, thereby reducing their binding affinities relative to IM2.

Similarly, as presented in Table 3, none of the library compounds demonstrated binding free energies or inhibition constants comparable to the control compound (4J6). Although C4, C20, C13 and C18 recorded the lowest free binding energies among the tested compounds, they were still significantly

less favourable compared 4J6. In addition, the superimposition of C4, C20, C13 and C18 revealed that these compounds adopted different orientations at the binding site compared to the control ligand 4J6. As illustrated in Figure 3 (a), C4 exhibited partial overlap and a slightly similar orientation to 4J6, which may have contributed to the formation of similar hydrogen bonding and hydrophobic interactions with key residues, accounting for its lowest binding energy (-6.47 kcal/mol) and favourable binding affinity to β-lactamase. In contrast, C20 and C13 adopted different orientations compared to 4J6, with their aliphatic side chains not aligning with the aliphatic chain of 4J6, as shown in Figures 3 (b) and (c), respectively. Figure 3 (d) showed that C18 had a partial overlap with 4J6, but its overall orientation differed significantly from 4J6, thus leading to poor alignment with critical interacting residues.

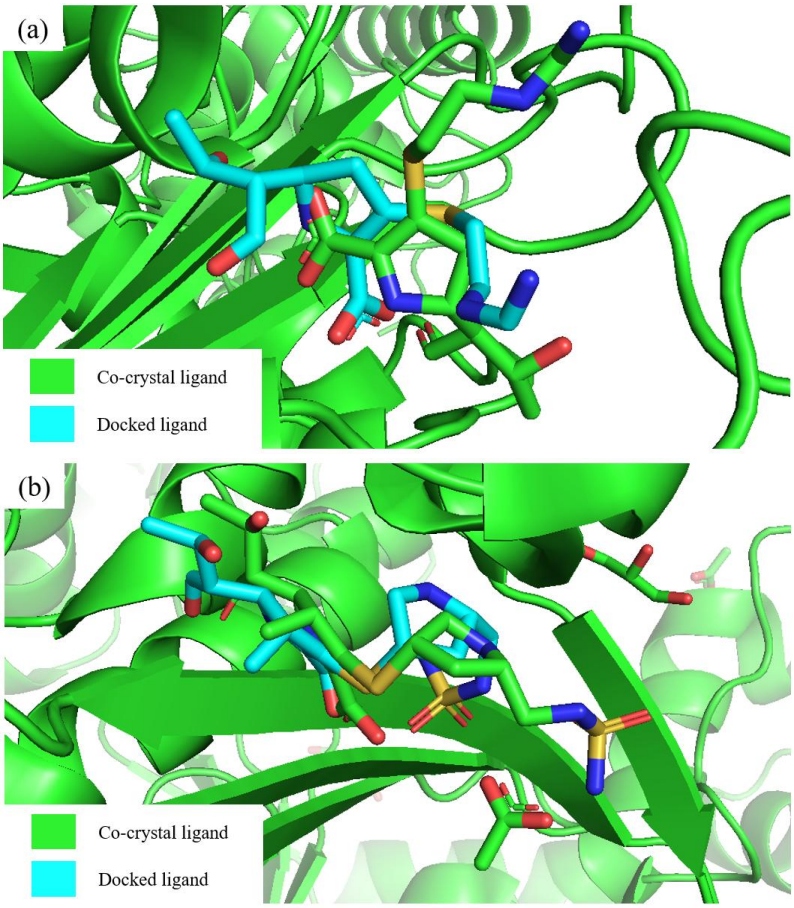

Figure 1 Superimposition between the best docking structure model (cyan) and original co-crystal ligand (green) for (a) IM2/PBP 1a complex and (b) 4J6/β-lactamase complex.

Table 2: Molecular docking results of tested ligands against PBP 1a (PDB ID: 3UDX).

Compound ID	Estimated binding free energy (kcal/mol)	Estimated inhibition constant, K_i (μM)
IM2 (control)	-6.05	36.81
C1	-3.48	2810.00
C2	-3.91	1360.00
C3	-3.73	1840.00
C4	**-5.36**	**118.27**
C5	-4.71	354.21
C6	-4.72	347.46
C7	-3.00	6290.00
C8	-3.82	1590.00
C9	-4.12	955.40
C10	-3.49	2780.00
C11	-4.32	680.61
C12	-3.62	2230.00
C13	**-5.24**	**145.38**
C14	-3.98	1210.00
C15	-4.25	767.58
C16	-2.77	9340.00
C17	-3.32	3690.00
C18	**-5.32**	**125.45**
C19	-3.15	4900.00
C20	**-5.65**	**72.11**

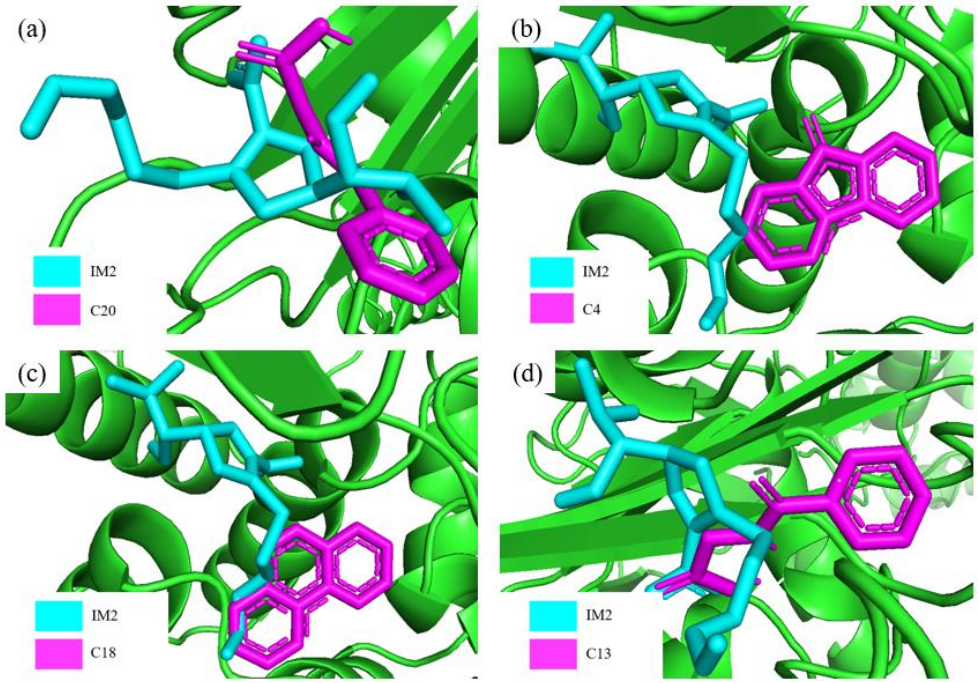

Figure 2 Superimposition of control ligand (IM2) with (a) C20, (b) C4, (c) C18, (d) C13 against PBP 1a.

Table 3: Molecular docking results of tested ligands against β-lactamase (PDB ID: 5L2F).

Compound ID	Estimated binding free energy (kcal/mol)	Estimated inhibition constant, K_i (nM)
4J6 (control)	-9.48	113.31
C1	-3.77	1740000.00
C2	-3.86	1480000.00
C3	-4.04	1100000.00
C4	**-6.47**	**17940.00**
C5	-4.88	265590.00
C6	-4.07	1050000.00
C7	-3.43	3060000.00
C8	-4.08	1020000.00
C9	-4.47	527120.00
C10	-3.46	2900000.00
C11	-4.49	511670.00
C12	-4.11	963520.00
C13	**-5.87**	**49890.00**
C14	-4.58	439340.00
C15	-4.14	918630.00
C16	-2.66	11210000.00
C17	-3.92	1330000.00
C18	**-5.62**	**76220.00**
C19	-4.05	1080000.00
C20	**-6.01**	**39410.00**

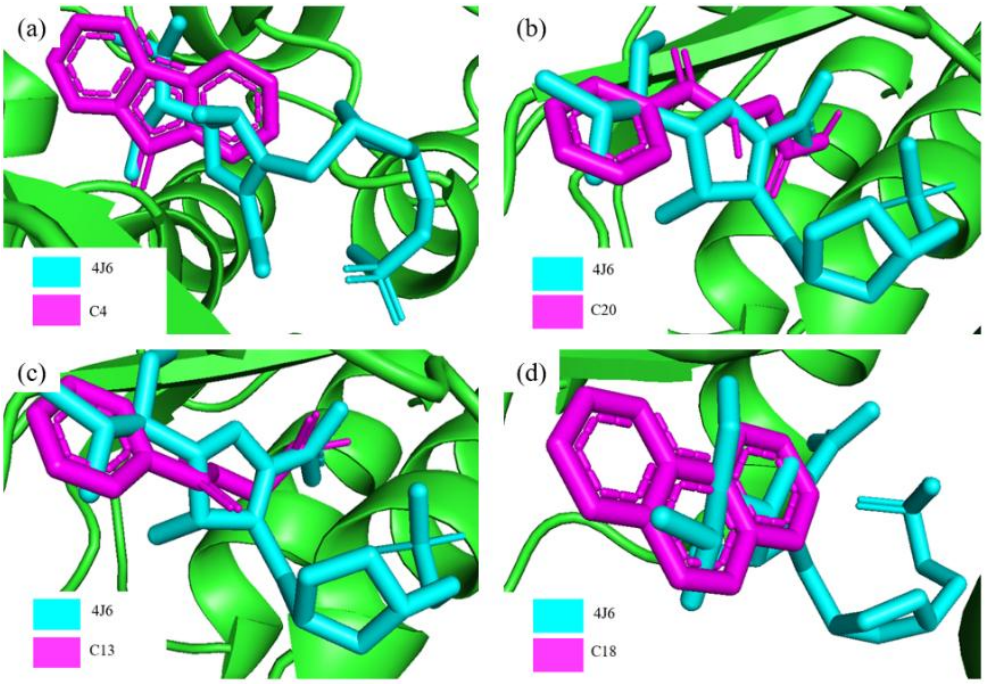

Figure 3 Superimposition of control ligand (4J6) with (a) C4, (b) C20, (c) C13, (d) C18 against β-lactamase.

Subsequent structure-activity relationship (SAR) analysis revealed that all selected compounds (C4, C13, C18 and C20) exhibited distinct hydrogen bonding networks and interaction patterns compared to IM2 and 4J6, likely due to differences in their functional groups or pharmacophore compositions. The binding profiles of the selected compounds against PBP 1a and β-lactamase were summarized in Tables 4 and 5, respectively.

According to Table 4, IM2 has polar functional groups such as imines (C=N), carbonyl (C=O) and carboxylate (COO^-) that serve as hydrogen bond acceptors in forming hydrogen bond interactions with the surrounding key residues. IM2 possessed the highest number of hydrogen bond acceptors, which enabled it to form the greatest number of hydrogen bonds with key active site residues. SAR analysis of C20 revealed it possessed functional groups such as amide (CONH), carboxyl (COOH), and a pyridine ring, allowing it to form interactions with several conserved residues of IM2, including SER434, SER487, LYS669, THR670, and GLY709, suggesting that it mimicked the binding behaviour of IM2. Meanwhile, C4 contained only one carbonyl (C=O) group, which allows it to form hydrogen bonds with SER434 and THR672. Furthermore, C18 possessed three aromatic rings (two pyridine rings fused with a central benzene ring) as well as two pyridine-like nitrogen atoms, which enable it to engage in hydrogen bonding, hydrophobic interactions, and π-lone pair interactions with SER470, SER487 and ASN489. C13 contains functional groups such as carbonyl (C=O), amide (CONH), and carboxyl (COOH), which can act as hydrogen bond donors and acceptors that interact with SER487, LYS669, THR672 and ASN674, as well as a pyridine ring capable of engaging in hydrophobic interactions with THR 672 and ALA676.

As shown in Table 5, 4J6 contains several polar functional groups, including carbonyl (C=O), carboxyl (COOH), hydroxyl (OH), and sulfamide (SO_2NH_2), as well as a pyrrolidine ring, which can serve as hydrogen bond donors and acceptors. The oxygen atoms on these functional groups allowed it to form hydrogen bonds with key amino acid residues such as SER80, SER127, SER218, TRP220, TRP222, ARG260, and ALA126. Furthermore, 4J6 also contains non-polar alkyl and sulfide (R-S-R') groups that contribute to forming hydrophobic interactions with PHE111, ILE129, LEU167, TRP220 and TRP222. Collectively, these polar and non-polar interactions enhanced the binding stability and affinity of 4J6 toward β-lactamase. The SAR analysis of C4 demonstrated that it consists of a carbonyl (C=O), a central five-membered ring and an aromatic benzene ring. These functional groups allowed C4 to form hydrogen bonds with SER80 and TRP220, and hydrophobic interactions with ALA79 and LEU167. Despite fewer interactions compared to 4J6, C4 exhibited the lowest binding free energy (-6.47 kcal/mol) and the highest predicted binding affinity among the selected compounds. This improved performance may be attributed to the formation of strong hydrogen bonds with critical residues within the active site. In addition, C20 contain functional groups such as pyridine-like nitrogen atom, amide (CONH), carboxyl (COOH) groups, and a pyridine ring, allowing it to form hydrogen bonds with SER80, GLY219, TRP220, TRP222 and ARG260. Although C13 shared the same functional groups as C20, it formed slightly different interactions with the key interacting residues at the active site of β-lactamase. It formed hydrogen bonds with SER80, SER127, SER218, TRP220 and ARG260, and hydrophobic interactions with ILE129 and TRP222. The SAR analysis of C18 revealed that it contains two pyridine-like nitrogen atoms and two fused pyridine rings connected via a central benzene ring. Surprisingly, despite the presence of nitrogen atoms that can serve as hydrogen bond acceptors, C18 did not form any hydrogen bonds with key active site residues, suggesting that the spatial orientation of C18 was not favourable for hydrogen bonding. Instead, C18 relied solely on hydrophobic interactions to interact with ALA79, LEU167 and TRP222. Consequently, this likely contributed to its comparatively weaker binding performance, as reflected by the highest binding free energy (-5.62 kcal/mol) and the lowest binding affinity among the four selected compounds.

Table 4: Binding profile of IM2 (control) and library compounds against PBP 1a (PDB ID: 3UDX).

Compound ID	Estimated binding free energy (kcal/mol)	Functional groups	Hydrogen bonds	Hydrophobic interactions	Electrostatic attraction
IM2 (Control)	-6.05	Imines (C=N), carbonyl (C=O) and carboxylate (COO^-)	SER434, SER470, ASP471, SER487, ARG488, LYS669, THR670, THR672, GLY709	-	LYS669
C4	-5.36	Carbonyl (C=O)	SER434, THR672	-	-
C13	-5.24	carbonyl (C=O), amide (CONH), carboxyl (COOH), pyridine ring	SER487, LYS669, THR672, ASN674	THR672, ALA676	-
C18	-5.32	Pyridine-like nitrogen atoms, pyridine and benzene rings	ASN489	SER470, SER487	-
C20	-5.65	Amide (CONH), carboxyl (COOH), and a pyridine ring	SER434, SER487, LYS669, THR670, GLY708, GLY709	TYR707	

Table 5: Binding profile of 4J6 (control) and library compounds against β-lactamase (PDB ID: 5L2F).

Compound ID	Estimated binding free energy (kcal/mol)	Functional groups	Hydrogen bonds	Hydrophobic interactions	Others (π-sulfur)
4J6 (Control)	-9.48	Carbonyl (C=O), carboxyl (COOH), hydroxyl (OH), and sulfamide (SO_2NH_2), pyrrolidine ring, alkyl, sulfide (R-S-R')	SER80, TRP114, ALA126, SER127, SER218, TRP220, TRP222, ARG260,	ILE129, LEU167, PHE111, TRP220, TRP222	TRP220
C4	-6.47	Carbonyl (C=O), central five-membered ring, benzene ring	SER80, TRP220	ALA79, LEU167	-
C13	-5.87	Pyridine-like nitrogen atom, amide (CONH), carboxyl (COOH), pyridine ring.	SER80, SER127, SER218, TRP220, ARG260	ILE129, TRP222	-
C18	-5.32	Pyridine-like nitrogen atoms, pyridine ring, benzene ring	-	ALA79, LEU167, TRP222	-
C20	-6.01	Pyridine-like nitrogen atom, amide (CONH), carboxyl (COOH), pyridine ring.	SER80, GLY219, TRP220, TRP222, ARG260	TRP222	

Following molecular docking and SAR analysis, C20 and C18 were selected for structural modification to enhance their binding affinities toward PBP 1a. C20 was chosen because it shared the most similar functional groups and key interactions with the control compound IM2, suggesting a favourable binding orientation. Although C18 did not exhibit the same key interactions as IM2, its binding profile indicated potential to form hydrogen bonds with nearby amino acid residues, making it a promising candidate for further optimization. On the other hand, C4 was selected as the sole compound for structural modification to enhance its binding affinity against β-lactamase. This decision was based on the fact that the binding free energy difference between 4J6 (the control) and C4 was the smallest among all library compounds, indicating the highest potential of C4 for further optimization. Moreover, although C4 did not possess the same functional groups as 4J6, the surrounding amino acid residues were highly similar, further supporting its suitability for structural modification. Based on these observations, it was hypothesized that incorporating similar substituents from control (IM2 and 4J6) into the structures of C20, C18 and C4 could increase the number of hydrogen bonds and hydrophobic interactions, thereby improving their binding affinity to PBP 1a and β-lactamase.

As depicted in Figure 4 (a), oriC20 (referred to as C20 previously) was modified by introducing functional groups such as imine (C=N), carboxylate (COO^-), and carbonyl (C=O) groups at positions C2, C8, and C10, respectively. An additional carboxylate (COO^-) group was also attached to the newly added imine group. Meanwhile, oriC18 (referred to as C18 previously) was modified by introducing functional groups such as carboxylate (COO^-), carbonyl (C=O), and amide ($CONH_2$) groups at atoms C1, C9, and C13, respectively, as illustrated in Figure 4 (b). As illustrated in Figure 4 (c), oriC4 (referred to as C4 previously) was modified by introducing functional groups such as carbonyl (C=O), sulfamide (SO_2NH_2), and carboxylate (COO^-) groups at positions C4, C15 and C17, respectively. The modified compounds (modC20, modC18 and modC4) were drawn using Avogadro software, and the resulting structures were subjected to redocking analysis against PBP 1a and β-lactamase to evaluate potential improvements in binding affinity. The redocking results revealed that all the modified compounds outperformed both the control and original compounds, as reflected by their lower binding free energies, as shown in Table 6. Subsequently, SAR analysis was performed to explore how specific structural modifications contributed to the enhanced interactions with the active site residues of PBP 1a and β-lactamase. The binding profiles of the modified compounds were summarized in Table 6.

The pharmacokinetics (PK) properties of the modified compounds (modC20, modC18 and modC4) were assessed based on the *in silico* ADMET (Absorption, Distribution, Metabolism, Excretion and Toxicity) prediction using the SwissADME server. As presented in Table 7, the modified compounds exhibited low gastrointestinal (GI) absorption, indicating their limited ability to permeate the intestinal membrane when administered orally. Furthermore, all three compounds were identified as non-substrates of P-glycoprotein (P-gp), a key ATP-binding cassette (ABC) transporter expressed in intestinal epithelial and cancer cells, which actively effluxes xenobiotics to protect the body from foreign substances (Alqahtani et al., 2021). This non-P-gp substrate nature of the modified compounds is considered favourable, as it suggests better intracellular retention and reduced susceptibility to efflux-mediated resistance. Additionally, all three compounds were predicted to be non-permeant to the blood-brain barrier (BBB), supporting their safety profile and specificity for non-central nervous system (CNS) infections. Notably, ADMET predictions indicated that none of the modified compounds inhibited CYP isoforms (CYP1A2, CYP2C19, CYP2C9, CYP2D6, and CYP3A4), suggesting minimal risk of CYP-mediated drug-drug interactions (DDI) or hepatic side effects (Zakaria et al., 2022). Among the modified compounds, modC18 exhibited the highest skin permeability with a Log Kp of -8.16 cm/s, followed by modC4 (-8.72 cm/s) and modC20 (-10.13 cm/s). These highly negative values suggest that none of the compounds are suitable for transdermal delivery, reinforcing the need for alternative administration routes, such as intravenous injection.

Meanwhile, Lipinski's rule of five (RO5) was employed to evaluate the druglike properties of these potential AMR counteragents. According to this rule, an ideal drug candidate should have a molecular weight (MW) < 500 g/mol, hydrogen bond acceptors (HBA) < 10, hydrogen bond donors

(HBD) < 5, and a calculated octanol-water partition coefficient (cLogP) value < 5. In addition, the topological polar surface area (TPSA) of a drug candidate should not exceed 140 $Å^2$. The druglikeness properties of the ligands presented in Table 8 showed that modC20 violated two of Lipinski's rule of five criteria, as it contains 10 hydrogen bond acceptors (HBA > 10) and 6 hydrogen bond donors (HBD > 5). Moreover, modC20 recorded the highest TPSA value (203.22 $Å^2$), significantly exceeding the recommended threshold of 140 $Å^2$ for optimal membrane permeability. Meanwhile, modC4 and modC18 recorded TPSA values of 172.24 $Å^2$ and 143.47 $Å^2$, respectively. Despite these deviations suggesting that the modified compounds would exhibit reduced membrane permeability and absorption, many drugs that violated the RO5 have still been approved by the FDA for clinical use as they demonstrated biological effectiveness and therapeutic potential (Houchi & Messasma, 2022). Furthermore, modC4 and modC18 recorded cLogP values of 0.14 and 0.47, respectively, indicating a favourable lipophilicity profile that supports sufficient membrane interaction without compromising solubility. In contrast, modC20 showed a cLogP value of -1.69, suggesting a highly hydrophilic nature. Therefore, modC18 and modC4 exhibited more desirable lipophilicity profiles for interacting with their respective targets, PBP 1a and β-lactamase.

Based on these findings, the ADMET and RO5 assessments indicated that none of the modified compounds are suitable for oral or transdermal delivery due to their poor GI absorption, low skin permeability, and high TPSA values. However, their favourable non-inhibition of CYP enzymes, non-P-gp substrate nature, and lipophilicity (except modC20) support their development as intravenous drugs for the treatment of multidrug-resistant *A. baumannii* infections. Overall, modC18 and modC4 emerged to be the most promising candidates targeting PBP 1a and β-lactamase, respectively.

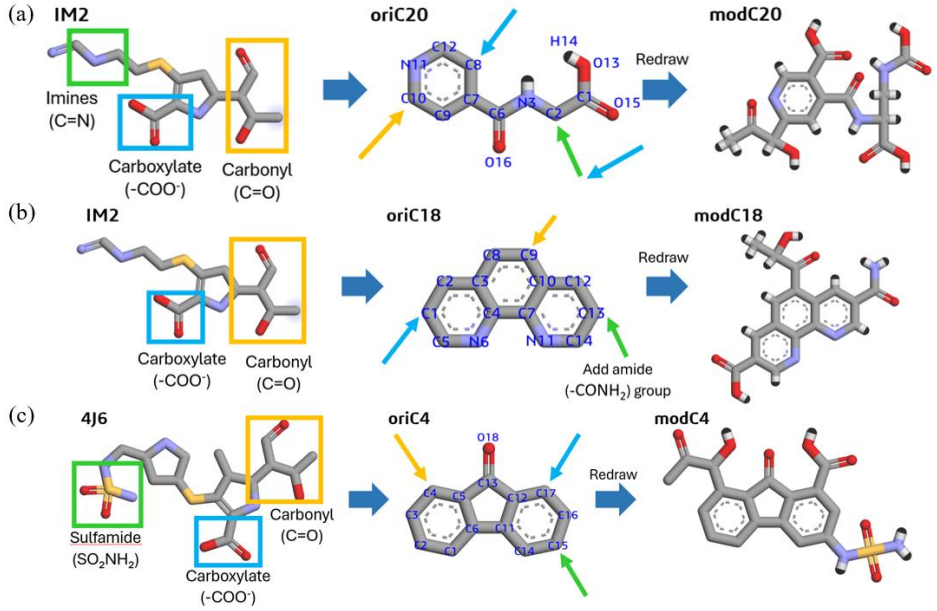

Figure 4 Structural modifications on (a) C20 and (b) C18 to improve binding affinity against PBP 1a and (c) C4 to improve binding affinity against β-lactamase.

Table 6: Binding profiles of modified compounds against PBP 1a and β-lactamase.

Compound ID	Estimated binding free energy (kcal/mol)	Hydrogen bonds	Hydrophobic interactions	Others (π-sulfur)
		PBP 1a		
modC20	-7.27	SER470, TYR485, SER487, LYS669, THR673, ASN674, ASP675, GLY709	THR672	
modC18	-8.72	SER470, ASP471, SER487, ARG488, ASN489, THR670, GLY709		
		β-lactamase		
modC4	-9.56	SER80, LYS125, ALA126, SER218, TRP220, TRP222, ARG260	PHE111, TRP114	PHE111, TRP114, TRP222

Table 7: Pharmacokinetics (PK) properties of modC20, mod C18 and modC4.

Compound ID	modC20	modC18	modC4
GI absorption	Low	Low	Low
BBB permeant	No	No	No
P-gp substrate	No	No	No
CYP1A2 inhibitor	No	No	No
CYP2C19 inhibitor	No	No	No
CYP2C9 inhibitor	No	No	No
CYP2D6 inhibitor	No	No	No
CYP3A4 inhibitor	No	No	No
Log K_p (skin permeation, cm/s)	-10.13	-8.16	-8.72

Table 8: The drug-likeness properties of modC20, modC18 and modC4.

Compound ID	modC20	modC18	modC4
Molecular weight (g/mol)	369.28	339.30	390.37
Number of hydrogen acceptors	10	7	8
Number of hydrogen donors	6	3	4
TPSA ($Å^2$)	203.22	143.47	172.24
cLogP	-1.69	0.47	0.14
Lipinski's violations	2	0	0

Conclusion

In conclusion, this study revealed that *in silico* computational tools were effective in identifying potential antimicrobial agents targeting PBP 1a and β-lactamase in *A. baumannii*. Although initial molecular docking and SAR analysis showed that most screened compounds did not outperform the control ligands (IM2 and 4J6) in terms of binding affinity, the interaction profiles provided valuable insights for the structural modification of compounds C4, C18, and C20 to improve their binding affinities toward both target proteins. Remarkably, redocking analysis of the modified compounds (modC4, modC18, and modC20) suggested that structural modification could enhance binding interactions, as reflected by their lower binding free energies compared to the original compounds. Subsequent *in silico* drug-likeness and ADMET predictions indicated that modC4 and modC18 were the most promising candidates for intravenous administration, targeting PBP 1a and β-lactamase, respectively, due to their

favourable pharmacokinetic properties and compliance with Lipinski's rule of five. In contrast, modC20 was less suitable due to violations of two Lipinski criteria.

Acknowledgement
This project was supported by the Faculty of Science, Universiti Teknologi Malaysia (UTM).

References

Alqahtani, M. S., Kazi, M., Alsenaidy, M. A., & Ahmad, M. Z. (2021). Advances in oral drug delivery. *Frontiers in Pharmacology, 12,* 618411.

De Oliveira, D. M., Forde, B. M., Kidd, T. J., Harris, P. N., Schembri, M. A., Beatson, S. A., Paterson, D. L., & Walker, M. J. (2020). Antimicrobial resistance in ESKAPE pathogens. *Clinical Microbiology Reviews, 33*(3), e00181-19.

Han, S., Caspers, N., Zaniewski, R. P., Lacey, B. M., Tomaras, A. P., Feng, X., Geoghegan, K. F., & Shanmugasundaram, V. (2011). Distinctive attributes of β-lactam target proteins in *Acinetobacter baumannii* relevant to development of new antibiotics. *Journal of the American Chemical Society, 133*(50), 20536–20545.

Houchi, S., & Messasma, Z. (2022). Exploring the inhibitory potential of *Saussurea costus* and *Saussurea involucrata* phytoconstituents against the Spike glycoprotein receptor binding domain of SARS-CoV-2 Delta (B.1.617.2) variant and the main protease (Mpro) as therapeutic candidates, using molecular docking, DFT, and ADME/Tox studies. *Journal of Molecular Structure, 1263,* 133032.

June, C. M., Muckenthaler, T. J., Schroder, E. C., Klamer, Z. L., Wawrzak, Z., Powers, R. A., Szarecka, A., & Leonard, D. A. (2016). The structure of a doripenem-bound OXA-51 class D β-lactamase variant with enhanced carbapenemase activity. *Protein Science, 25*(12), 2152–2163.

Ministry of Health Malaysia. (2022). *Malaysian action plan on antimicrobial resistance (MyAP-AMR) 2022–2026.* Ministry of Health Malaysia.

Naghavi, M., Vollset, S. E., Ikuta, K. S., Swetschinski, L. R., Gray, A. P., Wool, E. E., Aguilar, G. R., Mestrovic, T., Smith, G., Han, C., & Hsu, R. L. (2024). Global burden of bacterial antimicrobial resistance 1990–2021: A systematic analysis with forecasts to 2050. *The Lancet, 404*(10459), 1199–1226.

Tang, K. W. K., Millar, B. C., & Moore, J. E. (2023). Antimicrobial resistance (AMR). *British Journal of Biomedical Science, 80,* 11387.

Zakaria, M. Y., Georghiou, P. E., Banoub, J. H., & Beshay, B. Y. (2022). Inclusion of a phytomedicinal flavonoid in biocompatible surface-modified chylomicron mimic nanovesicles with improved oral bioavailability and virucidal activity: Molecular modeling and pharmacodynamic studies. *Pharmaceutics, 14*(5), 905.

Zango, U. U., Ibrahim, M., Shawai, S. A. A., & Shamsuddin, I. M. (2019). A review on β-lactam antibiotic drug resistance. *MOJ Drug Design Development & Therapy, 3*(2), 52–58.